Journal of Applied Polymer Science

SAXS Study on Deformation Behavior of Isotactic Polypropylene Under Pressurized CO_2

Noboru Osaka, Fumiya Kono, Hiromu Saito
Department of Organic and Polymer Materials Chemistry, Tokyo University of Agriculture and Technology, Koganei-Shi, Tokyo 184-8588, Japan
Correspondence to: N. Osaka (E-mail: osaka@cc.tuat.ac.jp)

ABSTRACT: Tensile-deformation behavior and structure change of isotactic polypropylene (iPP) under pressurized CO_2 were investigated by using *in situ* tensile-deformation instruments and small-angle X-ray scattering (SAXS) measurements. Tensile strength including yield stress, plateau stress, and tensile modulus decreased with increase of CO_2 pressure, suggesting that expansion of amorphous regions by absorbing CO_2 allows crystalline lamellae to deform easily with less entanglement. Under CO_2, the specimens became opaque beyond yield point and strong equatorial streaks appeared in two-dimensional SAXS patterns. By using Ruland's streak method, they are attributed to formation of nanometer-sized voids larger than the periodic distance of crystalline lamellae. An azimuthal profile of the lamellar peak was sharper under pressurized CO_2 than that under ambient pressure. This meant that the easy rotation of the crystalline lamellae by CO_2 results in the preferred orientation of the crystalline lamellae, which caused formation of the nanometer-sized voids at the interspace in the polymer matrix between lamellar stacks. Owing to the formation of the nanometer-sized voids, the elongation was enhanced in the second stage stretching of the stretched iPP at ambient pressure after depressurization. © 2012 Wiley Periodicals, Inc. J. Appl. Polym. Sci. 000: 000–000, 2012

KEYWORDS: polymer blends; SAXS; structure-property relations

Received 5 February 2012; accepted 9 March 2012; published online
DOI: 10.1002/app.37669

INTRODUCTION

Carbon dioxide (CO_2) can dissolve into amorphous polymers.[1] The dissolved CO_2 expands the molar volume of the amorphous polymers and then accelerates the molecular motion of the polymer.[2,3] Such a plasticization effect leads to dilation,[4] depression of glass transition temperature,[5,6] and decrease of viscosity.[7,8] In semicrystalline polymers, where a crystalline region coexists with an amorphous one, CO_2 is soluble in the amorphous region but insoluble inside the crystalline one due to the tight packing of the crystalline chain. In addition to the plasticization effect, depression of melting temperature is observed in semicrystalline polymers.[6,9–11] Our studies by the *in situ* dielectric relaxation spectroscopy[12] and light scattering (Kawate et al., manuscript in preparation), suggested that the plasticization of lamellar surface by CO_2 caused the depression of melting temperature. The insolubility of CO_2 into the crystalline region is also reflected on the exclusion of CO_2 during crystallization process.[13] The dissolved CO_2 in the molten state is excluded from the crystal growth front during the crystallization process and forms characteristic porous structures such as layered and rod-like ones.

Among the organic solvents, CO_2 have some advantages as both a plasticizer and a pressure transmitting media. When a system is depressurized, CO_2 escapes from the polymer substrate into the air, leaving no residual solvent. In contrast to the hydrostatic pressure effect by the organic solvents, with increase of CO_2 pressure, CO_2 is more absorbed into the polymer substrate and plasticizes the subject to a greater extent. With use of these specific properties of CO_2, CO_2 is widely used as a green and new solvent in polymer science.[14–16]

On the other hand, deformation is an important key in processing polymeric materials to produce strong physical properties. Many people have therefore investigated the deformation behavior to understand the strengthening mechanism for further improvement.[17–23] Especially, entanglement between polymers restricts the deformation of polymers, which leads to formation of the hierarchical structure. Because CO_2 is preferentially absorbed into the amorphous regions and expands the free volume, the entanglement

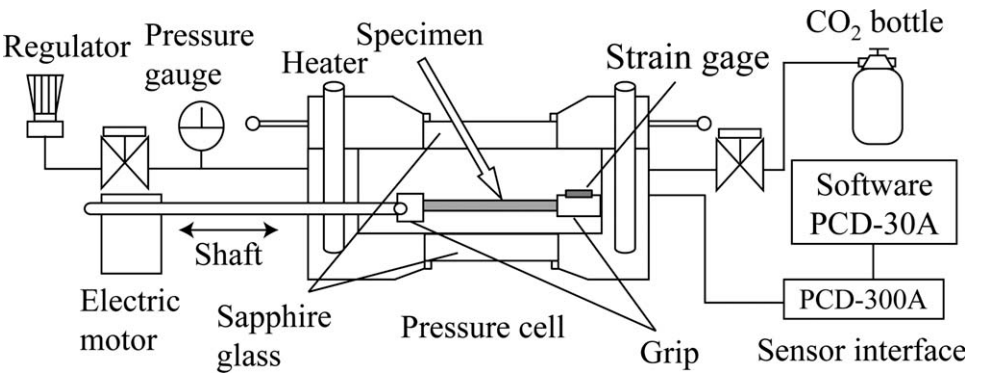

Figure 1. Schematic illustration of the instrumental setup for *in situ* stress-strain measurements under carbon dioxide.

is reduced under CO_2. Therefore, the semicrystalline polymers are expected to be easily deformed with less force under CO_2 and to form the specific hierarchical structure.

CO_2 is thus the promising plasticizer to produce the superior polymeric materials. Nevertheless, only a few studies were performed to reveal the effect of the plasticization of CO_2 on the drawing process of polymers, and the correlation between the deformation mechanism and the structure change during the stretching under CO_2 was not understood in detail.[24–26] In this study, to reveal the deformation behavior of the semicrystalline polymer under pressurized CO_2, we investigated the stress-strain behavior with the newly developed *in situ* tensile-deformation instrument and the structure change of isotactic polypropylene (iPP) in nano-ordered scale by small-angle X-ray scattering (SAXS). Here, iPP was chosen as the specimen because iPP is a well-studied polymer for its wide use in industry. The tensile-deformation behavior and structure change of iPP were discussed in terms of the plasticization effect of CO_2. The second stage stretching was also performed to understand the improved properties of the stretched iPP under CO_2.

EXPERIMENTAL

The iPP specimen used in this study was a commercial product (MA3Q, NOVATEC-PP) via a Ziegler-Natta catalyst supplied by Japan Polychem. The tacticity was 97% and the weight-average molecular weight was 2.5×10^5. The iPP powder was compression-molded between metal plates at 185°C for 5 min to obtain a film with the thickness of about 300 μm and then was quickly quenched in a water bath at room temperature. The alpha crystallographic phase of the iPP specimen is thus obtained.

To perform the *in situ* tensile-deformation measurements of the specimen under pressurized CO_2, we specially designed a stretching instrument for high-pressure experiment constructed of stainless steel (Taiatsu Techno, Japan), as shown in Figure 1. Two sapphire glass windows were mounted on the cell for through view. A crosshead of the elongational instrument (Taiatsu Techno, Japan) traveled at a speed of 30 mm/min in the high-pressure vessel. Movement of the crosshead was regulated by a shaft connected to a linear motor (Oriental Motor, Japan) outside the vessel. The shaft was passed through the special rubber of CHEMRAZ (Greene Tweed) to prevent the leakage of CO_2. A strain gage (KSN-2-120-E5-16 Kyowa Electronic Instruments, Japan) was attached to the surface of the crosshead to measure the stress during the stretching of the polymer film. During the measurement, electrical resistance of the strain gage was monitored by sensor interface PCD-30A. The obtained analog data was converted into digital data and recorded with a LabVIEW software.

A rectangular sample with a dimension of 10×30 mm^2 was cut from the iPP film for tensile deformation and mounted on a stretching instrument. After sealing, high-pressure CO_2 was injected into the cell with a syringe pump (NPKX-500, Nihon Seimitsu Kagaku, Japan) at room temperature and kept there for 1 h so that CO_2 would dissolve into the specimen. Then, the specimen was stretched. Further keeping time did not change the tensile properties. CO_2 pressure within the cell was monitored with an output pressure transducer and was kept constant with a back-pressure regulator (SCF-Bpg, Jasco, Japan). The temperature was set to be 35°C during this study with an autotune temperature controller unit in conjunction with a thermocouple. After elongation of the specimen up to an aimed strain, CO_2 was soon depressurized to ambient condition within 10 min. The stretched specimen thus obtained was used for SAXS, DSC, and second stage stretching measurements.

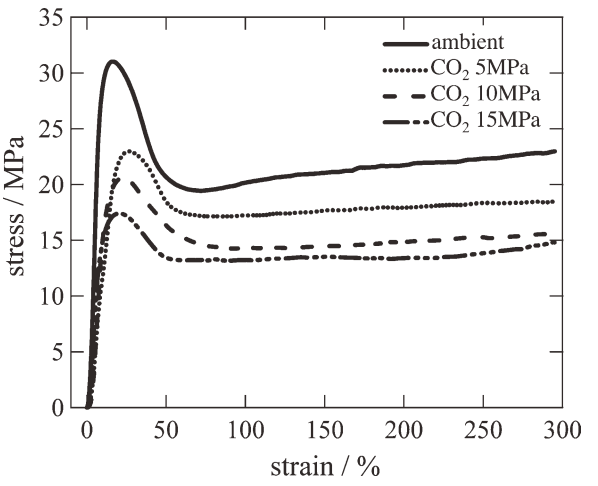

Figure 2. Stress-strain curves for the iPP specimens up to 300% without break at 35°C under various CO_2 pressures.

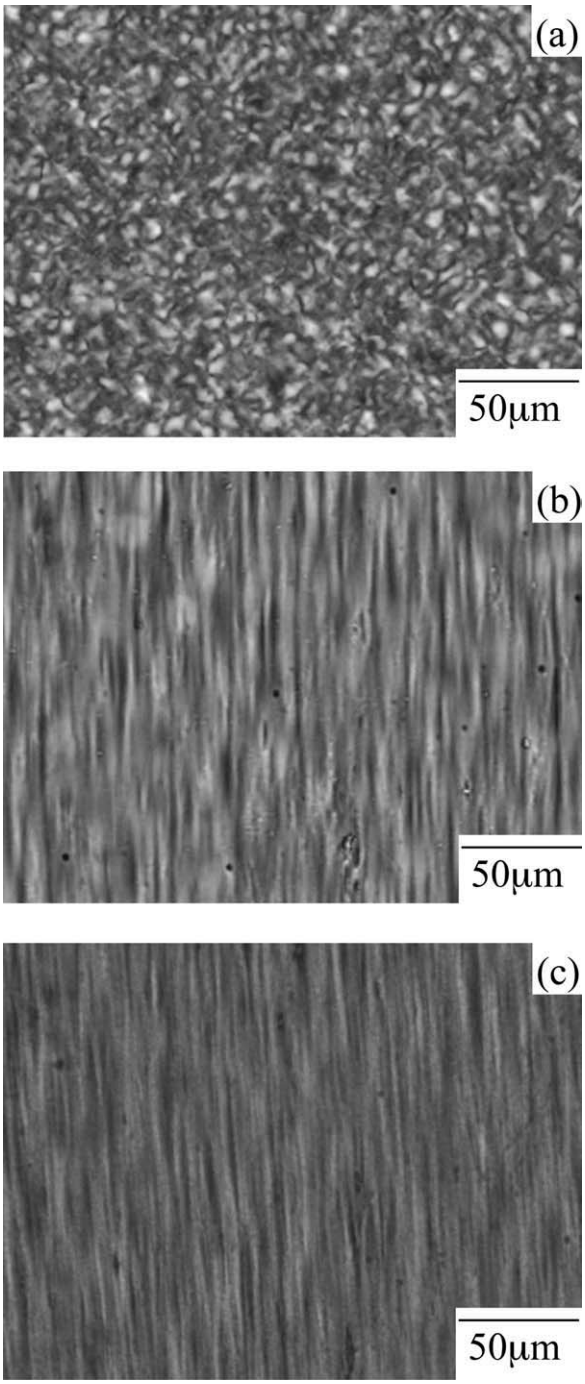

Figure 3. Photographs of the iPP specimens by polarized optical microscope at strains of (a) 0% and 300% under (b) ambient pressure, and (c) CO_2 of 10 MPa. The stretching direction is vertical.

SAXS measurements were performed by using NANO-Viewer system (Rigaku, Japan). A Cu-Ka radiation (46 kV, 60 mA) was generated and collimated by a confocal max-flux mirror system. The wavelength and the distance from sample to detector were 0.154 nm and 700 mm, respectively. An imaging plate (IP) (BAS-SR 127, Fujifilm, Japan) was used as a two-dimensional detector and the IP reading device (R-AXIS Ds3, Rigaku) was used to transform the obtained image into the text data. The exposure time was 3 h for each specimen. The scattering intensities were corrected with respect to the exposure time, the sample thickness, and the transmittance.

DSC measurements were conducted with a DSC8230 (Rigaku) at ambient pressure condition. The center of the deformed specimen was used for the DSC measurements. DSC scans were taken with a heating rate of 10°C/min. The second stretching was conducted at room temperature under air after preparing the stretched specimen for 6 months. Six months was sufficient to completely remove residual CO_2. Scattering data of the stretched iPP did not change during the period, which meant less structure relaxation of polymers or voids (data not shown). For the second stretching, a rectangular sample with a dimension of 5 × 7 mm^2 was cut from the central of the stretched specimen.

RESULTS AND DISCUSSION

Figure 2 shows stress-strain curves of the iPP film specimens under various CO_2 pressures obtained by the *in situ* tensile measurements up to a strain limit of 300% of the instrument without break. Tensile properties including tensile modulus, tensile stress, and yield stress decreased with increase of CO_2 pressure due to the plasticization effect of CO_2. Because CO_2 is insoluble inside the crystalline region due to the tight packing of the crystalline chain as reported in our previous study by *in situ* dielectric relaxation spectroscopy,[12] the dissolved CO_2 into the film expands only the amorphous region. This would reduce inner viscosity and entanglement in the amorphous region. The expanded amorphous region was therefore easily deformed with less force and hence the tensile strength decreased. With regard to the yield point, it first shifted toward higher strain as the CO_2 pressure increased. Expansion of amorphous region by absorbing CO_2 delayed the elongation needed for yielding up to 5 MPa. However, further application of CO_2 pressure above 10 MPa inverted the shift of the yield strain to lower strain although other tensile properties monotonically decreased with increase of CO_2 pressure. As the CO_2 pressure increases, a larger amount of CO_2 is absorbed into the iPP specimen[27] and the crystalline lamellae obtain larger free volume to deform. Therefore, the crystalline lamellae could easily deform with less entanglement and force by absorbing a larger amount of CO_2 and the yield strain decreased.

Figure 3 shows polarized optical micrographs of the iPP specimen obtained by stretching at different strains under various CO_2 pressures. Before stretching, small spherulites with the radius of 10 μm were observed. The spherulites of iPP were completely destroyed and transformed to the fibrillar morphologies aligned in the stretching direction after the yielding. It seems that each bundled fibril obtained under CO_2 pressure of 10 MPa are well oriented in the stretching direction. Hereafter, to understand the deformation behavior and structure change of iPP under CO_2 in detail, we performed SAXS measurements on the iPP specimens at various strains.

Figure 4 shows two-dimensional SAXS patterns of iPP specimen stretched at different strains under various CO_2 pressures. Before stretching, a circularly isotropic SAXS pattern indicates

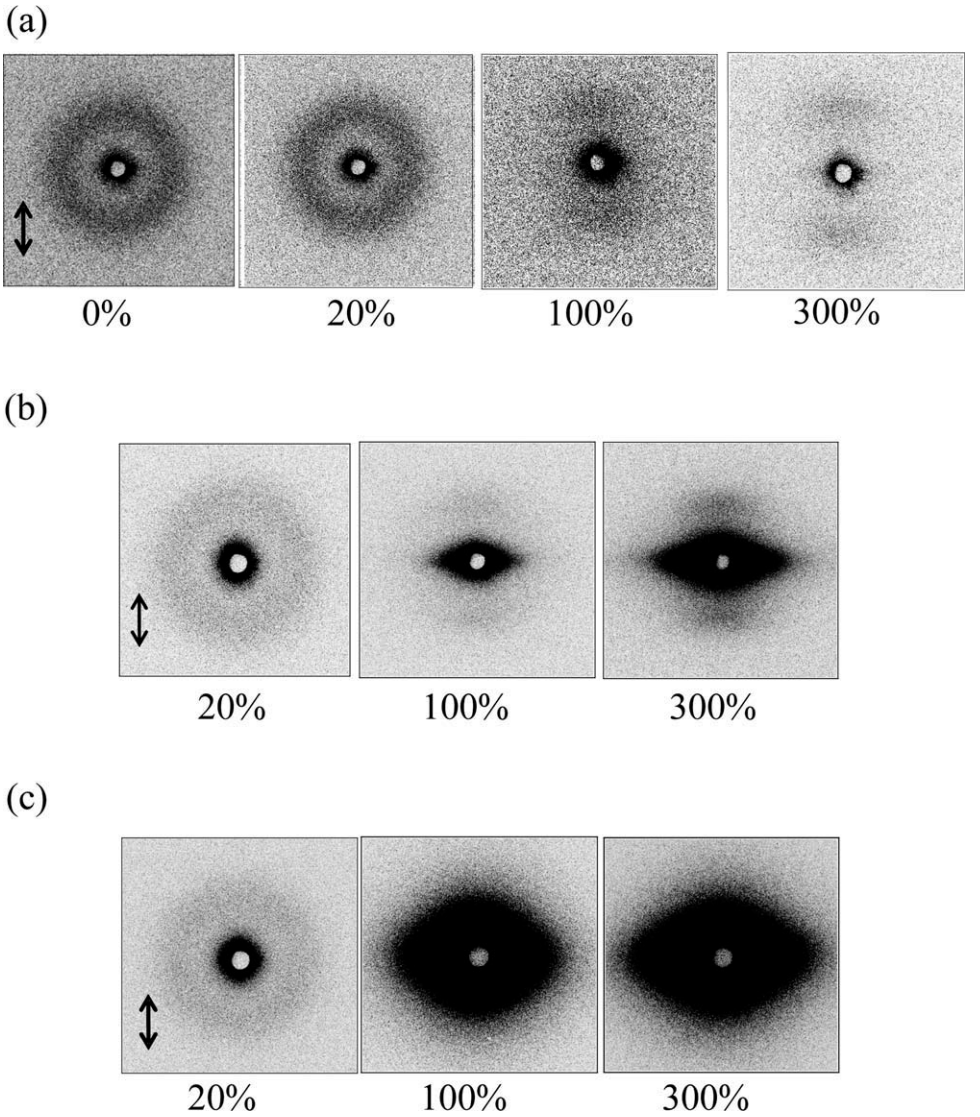

Figure 4. Two-dimensional SAXS patterns taken at different deformations at 35°C under (a) ambient pressure, (b) CO_2 of 5 MPa, and (c) CO_2 of 10 MPa. Stretching direction was vertical as shown by the two-head arrow.

random orientation of nanometer-sized crystalline lamellae. At a strain of 20% just before yielding, no clear change of the SAXS pattern was observed. At a strain of 100% after the yield point, the maximum spot was observed in the meridional direction, suggesting that the crystalline lamellae were rotated and oriented in the stretching direction. However, under pressurized CO_2 of 5 MPa, in addition to the oriented scattering pattern from the lamellae, a strong equatorial streak appeared at a strain of 100%. Further strain to 300% lead to enlargement of the equatorial streak. Such an equatorial streak is usually derived from cross-section of fibrils or voids. The origin of the equatorial streak is described in the following.

The iPP specimens were almost transparent before stretching due to the low degree of crystallinity and they kept transparent by stretching beyond the yield point under ambient pressure. However, they became opaque beyond the yield point under pressurized CO_2. They were investigated by density measurements as shown in Table I. At ambient pressure, density of the specimen did not change by stretching. However, it decreased by about 10% by stretching under pressurized CO_2 of 5 MPa. Further decrease was seen with increase of CO_2 pressure up to 10 MPa. This result strongly suggests that voids are formed by stretching under pressurized CO_2 and weight fraction of the void in the specimen increased with increase of CO_2 pressure.

Table I. Properties of the iPP Specimen Taken at Various CO_2 Pressures and Strains

	0	0	5	10
CO_2 pressure/MPa strain/%	0	300	300	300
specific gravity/g cm^3	0.926	0.927	0.827	0.807
crystallinity/%	39.1	55.5	52.0	53.0
T_m/°C	163.5	163.7	162.9	163.5

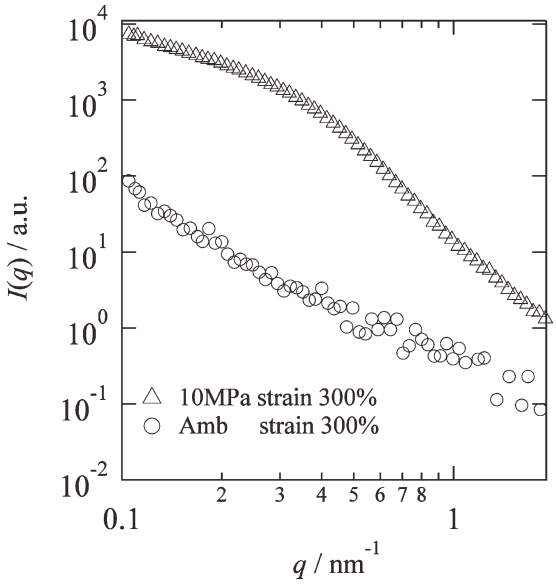

Figure 5. One-dimensional scattering curves in the equatorial direction of two-dimensional SAXS pattern in Figure 3 at different CO_2 pressures.

Figure 5 shows the one-dimensional scattering curves in the equatorial direction of the two-dimensional scattering pattern shown in Figure 4. A large difference of the scattering intensity by two orders of magnitude is observed between the stretched specimens under air and pressurized CO_2. The large difference is ascribed to electron density difference between the scattering objects and the matrix. The scattering intensity depends on the square of the electron density difference. Because the electron density of voids is zero value, void formation in the fibril under pressurized CO_2 enhanced the electron density difference between the scattering objects and the matrix, which then caused the increase in the scattering intensity to a greater extent. To characterize the scattering object observed in the SAXS patterns, the intensity distribution of the equatorial streak was analyzed by using the so called Ruland's method.[28–33] In

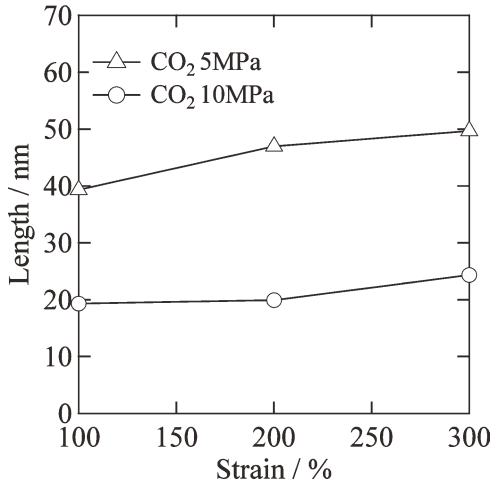

Figure 6. Strain dependence of length of voids obtained by Ruland's streak method under different CO_2 pressures.

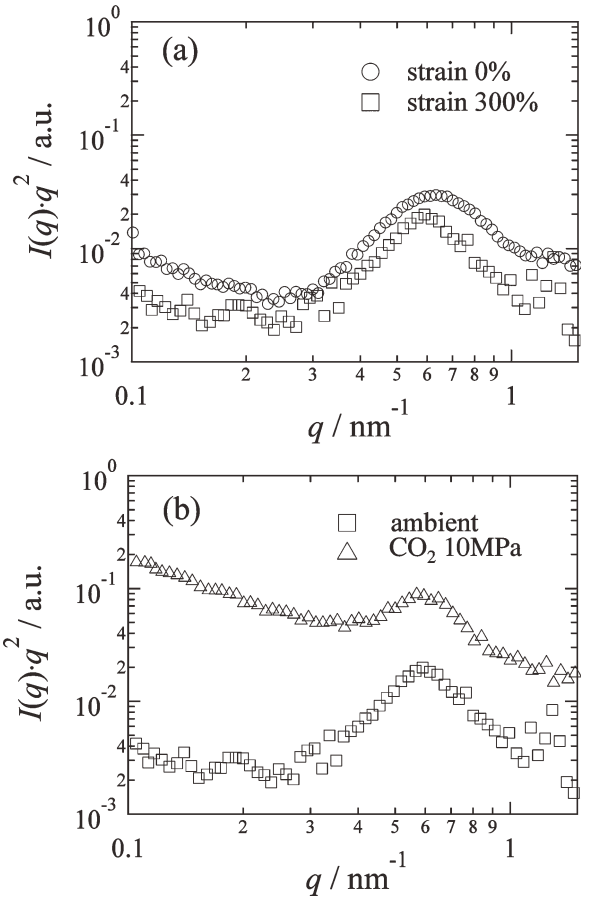

Figure 7. Lorentz-corrected one-dimensional scattering curves in the meridional direction of two-dimensional SAXS pattern in Figure 3 (a) at various strains under ambient pressure and (b) at a strain of 300% under CO_2 pressure of 10 MPa.

Ruland's method, the oriented 2D SAXS pattern such as streak is considered. The integral width of the equatorial streak in reciprocal space corresponds to the inverse length of the void in real space. To reduce contribution from lamellar peak for the

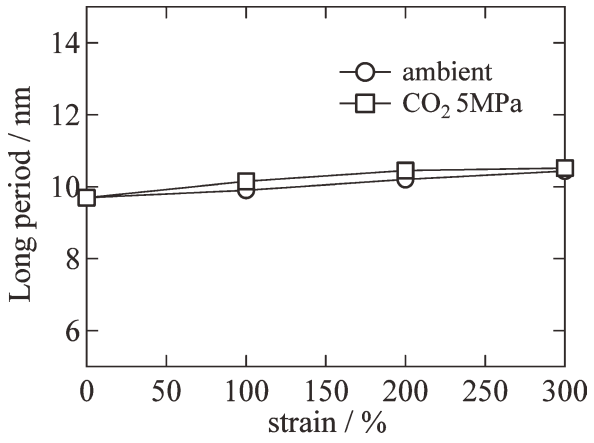

Figure 8. Strain dependence of lamellar periodic distance at different CO_2 pressures.

Table II. Strain Dependence of Void Length and Lamellar Periodic Distance Under Various CO_2 Pressures, Respectively

CO_2 pressure (MPa)	Strain (%)	Void Length (nm)	Lamellar periodic distance (nm)
0	0		9.7
0	100		9.9
0	200		10.2
0	300		10.4
5	100	39.2	10.1
5	200	47.0	10.4
5	300	50.5	10.5
10	100	19.6	
10	200	20.1	
10	300	24.2	

integral, we adopted slice integration parallel to the meridian direction instead of azimuthal integration.[33] The slice distributions at different q along the equator were fitted with Patterson VII function, which lead to the following equation

$$B_{s3} \approx \frac{1}{l_f} + qB_\phi$$

where B_{s3} is the slice integral breadth, l_f is the effective length of the void in the stretching direction, and B_ϕ is the misorientation width of the void. We can obtain l_f from the extrapolated intercept at $q = 0$.

Figure 6 shows strain dependence of l_f at various CO_2 pressures. The obtained values of l_f are several dozen nanometers and much shorter than length of the fibrils of micrometer scale as shown in Figure 3. This result strongly suggests that the equatorial streak seen in SAXS patterns originates from the nanometer-sized voids and not from the fibrils. With increase of strain, the void length in the stretching direction increased. The change of the void length did not follow the affine deformation. Beyond the yielding point, stretched polymers are transformed into fibrils and interlamellar amorphous region are entangled.

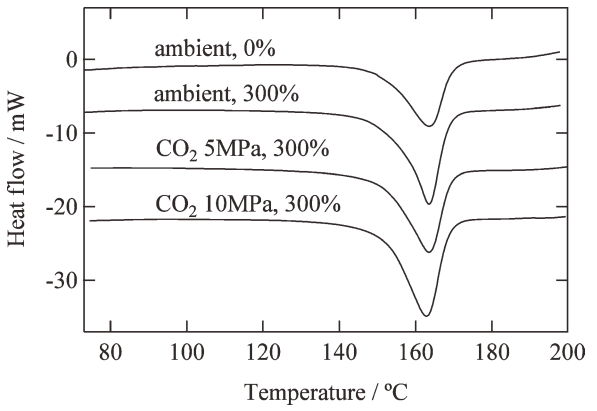

Figure 9. DSC scans of the stretched iPP films up to a strain of 300% under various CO_2 pressures at a scanning rate of 10°C/min.

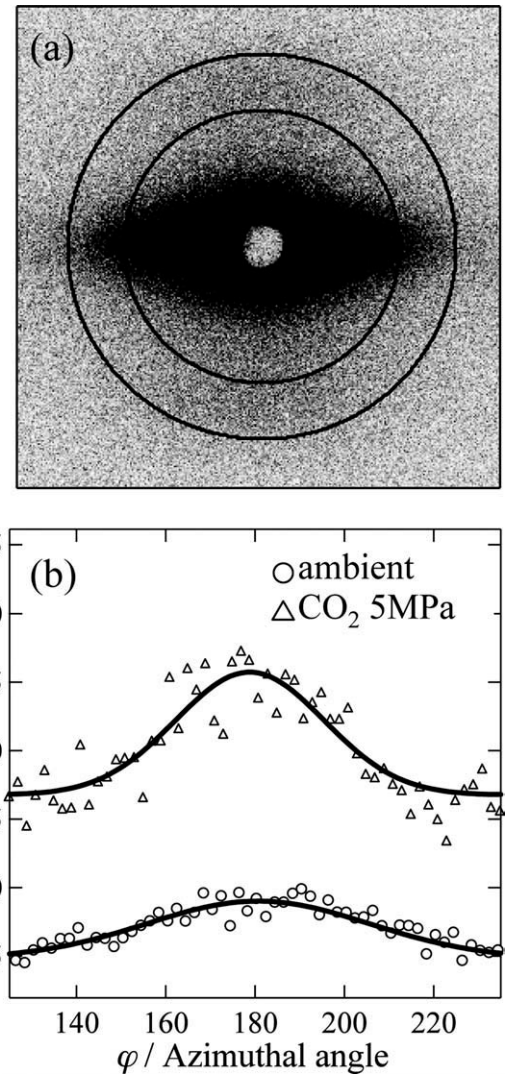

Figure 10. (a) An azimuthally scanned area encircled by double circle in two-dimensional SAXS pattern and (b) azimuthal profile of the lamellar peak at a strain rate of 300% under various CO_2 pressures. The solid lines are guide for eyes fitted by Gaussian functions.

Because the void length is determined by the surrounding complicated structures, their changes prevented the affine deformation of the voids. However, with increase of CO_2 pressure, the void length was decreased. Because higher pressure increases the amount of CO_2 dissolving into the specimen at these pressure ranges, more voids would be generated. It is therefore considered that existence of more voids in the specimen at higher pressure prevented elongation of the voids.

In order to understand the plasticization effect of CO_2 on the lamellar periodic distance, the one-dimensional scattering intensity in the meridional direction in Figure 4 was multiplied by square of q for the data treatment (Lorentz correction).[34–36] Figure 7 shows Lorentz-corrected one-dimensional scattering curves in the meridional direction at various strains under ambient pressure and at a strain of 300% under CO_2 pressure of 10 MPa. A broad peak indicating the lamellar periodic distance

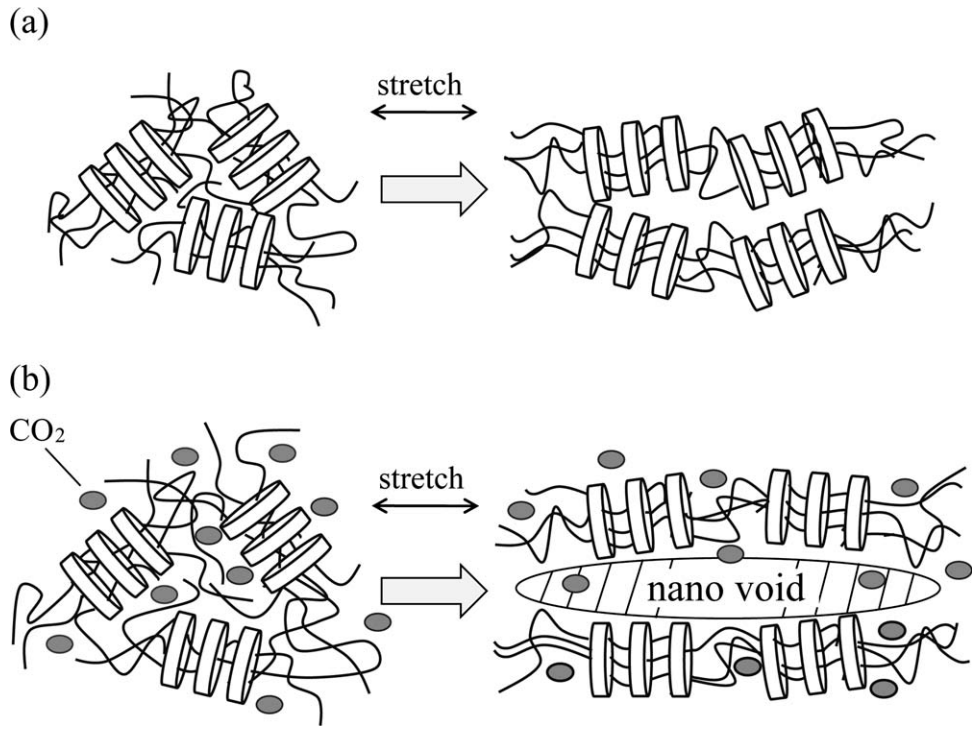

Figure 11. Schematics of deformation and void formation for the iPP specimen under (a) ambient pressure and (b) CO_2 pressure.

is seen. At ambient pressure, no distinctive change of the scattering profile is observed. However, upturn of the scattering intensity at low q region is observed at CO_2 pressure of 10 MPa. This upturn is caused by the appearance of the streak pattern because of the void formation mentioned before. However, only a slight shift of the peak position toward lower q is observed up to a strain of 300% irrespective of CO_2 pressure.

Figure 8 shows strain dependence of the lamellar periodic distance at different CO_2 pressures. The lamellar periodic distance was about 10 nm and slightly increased with increase of strain irrespective of CO_2 pressure. These values and the obtained void lengths under various strains and CO_2 pressures are summarized in Table II. Compared with the drastic decrease in the tensile strength as shown in Figure 2, the plasticization effect of CO_2 had less influence on the structure change of the crystalline lamella by stretching. In addition, it should be also noted that they are smaller than the void length. It is therefore considered that the nanometer-sized voids were formed at the interspace in the polymer matrix between lamellar stacks and not inside the lamellar stacks.

Crystallinity of the stretched specimen was evaluated by DSC. Figure 9 shows DSC scans of the stretched iPP films up to a strain of 300% under various CO_2 pressures. The endothermic peak became sharper and larger by stretching whereas the position of the melting peak did not change. Because melting temperature is predominantly correlated with thickness of the crystalline lamella,[37,38] this is consistent with the SAXS result that the increase of the lamellar periodic distance was only 10% up to a strain of 300% irrespective of CO_2 pressure. Table I shows that stretching of the iPP specimen up to a strain of 300% caused to increase the crystallinity by about 15%, but the significant pressure dependence was not observed. It is therefore concluded that stretching of the iPP specimen up to a strain of 300% at 35°C only lead to increase in fraction of the crystalline component irrespective of CO_2 pressure.

To understand the orientational degree of the crystalline lamellae under pressurized CO_2, we evaluated broadness of the azimuthal profile of lamellar peak in an encircled area indicated by double circle in two-dimensional SAXS pattern as shown in Figure 10(a). Figure 10 (b) shows that the azimuthal profile of the lamellar peak is sharper under CO_2 of 5 MPa than that under ambient pressure. The result means that the crystalline lamellae are well oriented in the stretching direction under pressurized

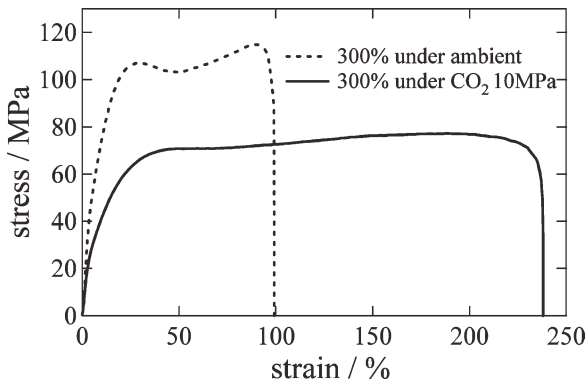

Figure 12. Second stage stretching of the iPP specimen stretched up to a strain rate of 300% under various CO_2 pressures.

CO_2. Because CO_2 cannot dissolve into the crystalline lamellae,[11] the amorphous region surrounding the crystalline phase was expanded by absorbed CO_2. The crystalline lamellae were therefore easily rotated because of the reduced entanglement by the plasticization effect of CO_2 and hence well oriented in the stretching direction.

Beyond the yield point, the crystalline lamellae are oriented in the stretching direction and the spherulite is transformed into the fibril. Under pressurized CO_2, because the amorphous region is expanded by absorbed CO_2, the crystalline lamellae were easily and well oriented in the stretching direction as a result of the reduced entanglement. In addition, as mentioned above, SAXS measurements also revealed that the void length of several dozen nanometers was larger than the lamellar periodic distance of about 10 nm. Therefore, the voids were formed at interspace between well-oriented lamellar stacks but not inside the lamellae stacks during the orientation of the lamellar stacks by stretching under pressurized CO_2. However, when degree of orientation is low, the crystalline lamellae are overlapped each other to some extent. Therefore, the predominant nanometer-sized voids do not appear at ambient pressure. The schematic for deformation and void formation is illustrated in Figure 11.

To understand the effect of the structure change on the mechanical property, the stretched specimens up to a strain of 300% were stretched again at ambient pressure after preparing the stretched specimens for 6 months. Figure 12 shows tensile-deformation behavior of the iPP specimen in the second stage stretching. The tensile strength of the deformed iPP films was more than 200% larger compared with that in the first stretching stage shown in Figure 2. This enhanced tensile strength is ascribed to the increased crystallinity and orientation of crystalline lamellae along the stretching direction in the first stretching stage. However, there is a large difference in the tensile strength between the deformed iPP film under ambient pressure and CO_2 pressure. SAXS measurements revealed that nanometer-sized voids were formed in the iPP specimen during the stretching process under CO_2. Existence of the nanometer-sized voids offered extra space for easy deformation with less force. Therefore, lower tensile strength of the CO_2-treated iPP than untreated one is attributed to presence of the nanometer-sized voids in the fibrils. In addition, maximum strain of the iPP specimen stretched under pressurized CO_2 of 10 MPa was more than twice the one obtained under air at ambient pressure, suggesting that the CO_2 treated iPP had better drawability than one obtained under air due to suppression of the stress concentration by the nanometer-sized voids. With respect to the yielding behavior, the yielding point did not appear in the stretched film obtained under pressurized CO_2. Because the orientational degree of the crystalline lamellae in the stretched iPP under pressurized CO_2 was enough high as revealed by SAXS, the crystalline lamellae did not afford to rotate in the stretching direction, which suppressed the yielding behavior.

CONCLUSION

Stress-strain behavior and structure change of iPP film under pressurized CO_2 were investigated by *in situ* tensile-deformation instrument and SAXS. With increase of CO_2 pressure, tensile strength such as yielding stress and plateau stress was monotonically decreased. CO_2 is only absorbed into amorphous region and amount of the absorption is increased by applying CO_2 pressure at the measured region. Expansion of the amorphous region therefore allowed crystalline lamellae to deform with less entanglement. It was found that the stretched film under pressurized CO_2 became opaque. Strong equatorial streaks appeared beyond the yielding point in two-dimensional SAXS pattern of the stretched film under pressurized CO_2. This suggests formation of nanometer-sized voids in the film, which highly reflected the light. Azimuthal profiles of the lamellar peak in two-dimensional SAXS pattern showed that the crystalline lamellae were well oriented in the stretching direction under pressurized CO_2 due to the plasticization effect of CO_2 on the surrounding amorphous region. Such characteristic structure obtained by stretching under pressurized CO_2 affects on the mechanical property of the second stage stretching. The existence of the nanometer-sized voids increased drawability of the stretched films more than twice one without the voids due to extra space for deformation and highly oriented crystalline lamellae obtained by stretching under pressurized CO_2 suppressed the yielding behavior.

ACKNOWLEDGMENTS

This work was partially supported by the Japan Society for the Promotion of Science (Grant-in-Aid for Scientific Research, No. 20350101).

REFERENCES

1. Kazarian, S. G. *Polym. Sci. Ser. C* **2000,** *42*, 78.
2. Matsumiya, Y.; Inoue, T.; Iwashige, T.; Watanabe, H. *Macromolecules* **2009,** *42*, 4712.
3. Neyertz, S.; Brown, D.; van der Vegt, N. F. A. *Macromolecules* **2010,** *43*, 7813.
4. Goel, S. K.; Beckman, E. *J. Polymer* **1993,** *34*, 1410.
5. Shieh, Y.-T.; Su, J.-H.; Manivannan, G.; Lee, P. H. C.; Sawan, S. P.; Spall, W. D. *J. Appl. Polym. Sci.* **1996,** *59*, 707.
6. Zhang, Z.; Handa, Y. P. *Macromolecules* **1997,** *30*, 8505.
7. Bae, Y. C.; Gulari, E., *J. Appl. Polym. Sci.* **1997,** *63*, 459.
8. Areerat, S.; Nagata, T.; Ohshima, M. *Polym. Eng. Sci.* **2002,** *42*, 2234.
9. Handa, Y. P.; Zhang, Z.; Wong, B. *Macromolecules* **1997,** *30*, 8499.
10. Shenoy, S. L.; Fujiwara, T.; Wynne, K. *J. Macromolecules* **2003,** *36*, 3380.
11. Legrand, D. G. *J. Appl. Polym. Sci.* **1969,** *13*, 2129.
12. Yamamura, Y.; Yoshida, K.; Kawate, K.; Osaka, N.; Saito, H. *Polym. J.* **2010,** *42*, 419.
13. Koga, Y.; Saito, H. *Polymer* **2006,** *47*, 7564.
14. Cooper, A. I. *J. Mater. Chem.* **2000,** *10*, 207.
15. Xu, Q.; Pang, M.; Peng, Q.; Li, J.; Jiang, Y. *J. Appl. Polym. Sci.* **2004,** *94*, 2158.

16. Nalawade, S. P.; Picchioni, F.; Janssen, L. P. B. M. *Prog. Polym. Sci.* **2006,** *31*, 19.
17. Butler, M. F.; Donald, A. M. *Macromolecules* **1998,** *31*, 6234.
18. Zhang, X. C.; Butler, M. F.; Cameron, R. E. *Polymer* **2000,** *41*, 3797.
19. Ran, S.; Zong, X.; Fang, D.; Hsiao, B. S.; Chu, B.; Phillips, R. A. *Macromolecules* **2001,** *34*, 2569.
20. Shioya, M.; Kawazoe, T.; Kojima, J.; Sakurai, S.; Yamamoto, K.; Kikutani, T. *Polymer* **2006,** *47*, 3616.
21. Nozue, Y.; Shinohara, Y.; Ogawa, Y.; Sakurai, T.; Hori, H.; Kasahara, T.; Yamaguchi, N.; Yagi, N.; Amemiya, Y. *Macromolecules* **2007,** *40*, 2036.
22. Pawlak, A.; Galeski, A. *Macromolecules* **2008,** *41*, 2839.
23. Chae, H. G.; Kumar, S. *Science* **2008,** *319*, 908.
24. Hobbs, T.; Lesser, A. J. *J. Polym. Sci. Part B: Polym. Phys.* **1999,** *37*, 1881.
25. Hobbs, T.; Lesser, A. *J. Polymer* **2000,** *41*, 6223.
26. Hobbs, T.; Lesser, A. *J. Polym. Eng. Sci.* **2001,** *41*, 135.
27. Saito, Y.; Fujiwara, K.; Takikawa, T.; Sumarno; Takishima, S.; Masuoka, H. *Polymer* **1999,** *162*, 261.
28. Ruland, W. *J. Polym. Sci. Part C* **1969,** *28*, 143.
29. Thünemann, A. F.; Ruland, W. *Macromolecules* **2000,** *33*, 1848.
30. Keum, J. K. B. C.; Hsiao, B. S.; Somani, R.; Yang, L.; Chu, B.; Kolb, R.; Chen, H.; Lue, C.-T. *Prog. Colloid Polym. Sci.* **2005,** *130*, 114.
31. Tang, Y.; Jiang, Z.; Men, Y.; An, L.; Enderle, H.-F.; Lilge, D.; Roth, S. V.; Gehrke, R.; Rieger, J. *Polymer* **2007,** *48*, 5125.
32. Keum, J. K.; Zuo, F.; Hsiao, B. S. *Macromolecules* **2008,** *41*, 4766.
33. Wang, W.; Murthy, N. S.; Chae, H. G.; Kumar, S. *J. Polym. Sci. Part B: Polym. Phys.* **2009,** *47*, 2394.
34. Cser, F. *J. Appl. Polym. Sci.* **2001,** *80*, 358.
35. Cser, F. *J. Appl. Polym. Sci.* **2001,** *80*, 2300.
36. Cser, F.; Hopewell, J. L.; Shanks, R. A. *J. Appl. Polym. Sci.* **2001,** *81*, 340.
37. Supaphol, P. *J. Appl. Polym. Sci.* **2001,** *82*, 1083.
38. Stern, C.; Frick, A.; Weickert, G. *J. Appl. Polym. Sci.* **2007,** *103*, 519.